



CHORUS

This is the accepted manuscript made available via CHORUS. The article has been published as:

Prediction of high-math
 μTc superconductivity in
ternary lanthanum borohydrides

Xiaowei Liang, Aitor Bergara, Xudong Wei, Xiaoxu Song, Linyan Wang, Rongxin Sun,
Hanyu Liu, Russell J. Hemley, Lin Wang, Guoying Gao, and Yongjun Tian

Phys. Rev. B **104**, 134501 — Published 4 October 2021

DOI: [10.1103/PhysRevB.104.134501](https://doi.org/10.1103/PhysRevB.104.134501)

Prediction of high- T_c superconductivity in ternary lanthanum borohydrides

Xiaowei Liang,¹ Aitor Bergara,^{2,3,4} Xudong Wei,¹ Xiaoxu Song,¹ Linyan Wang,¹ Rongxin Sun,¹ Hanyu Liu,^{5,6,*} Russell J. Hemley,⁷ Lin Wang,¹ Guoying Gao,^{1,†} and Yongjun Tian¹

¹*Center for High Pressure Science, State Key Laboratory of Metastable Materials Science and Technology, Yanshan University, Qinhuangdao 066004, China*

²*Departamento de Física de la Materia Condensada, Universidad del País Vasco, UPV/EHU, 48080 Bilbao, Spain*

³*Donostia International Physics Center (DIPC), 20018 Donostia, Spain*

⁴*Centro de Física de Materiales CFM, Centro Mixto CSIC-UPV/EHU, 20018 Donostia, Spain*

⁵*International Center for Computational Method & Software and State Key Laboratory of Superhard Materials, College of Physics, Jilin University, Changchun 130012, China*

⁶*Key Laboratory of Physics and Technology for Advanced Batteries (Ministry of Education), International Center of Future Science, Jilin University, Changchun 130012, China*

⁷*Departments of Physics and Chemistry, University of Illinois at Chicago, Chicago IL 60607, USA*

(Dated: September 20, 2021)

The study of superconductivity in compressed hydrides is of great interest due to measurements of high critical temperatures (T_c) in the vicinity of room temperature, beginning with the observations of LaH₁₀ at 170-190 GPa. However, the pressures required for synthesis of these high T_c superconducting hydrides currently remain extremely high. Here we show the investigation of crystal structures and superconductivity in the La-B-H system under pressure with particle-swarm intelligence structure-searches methods in combination with first-principles calculations. Structures with seven stoichiometries, LaBH, LaBH₄, LaBH₆, LaBH₇, LaBH₈, La(BH)₃ and La(BH₄)₃ were predicted to become stable under pressure. Remarkably, the hydrogen atoms in LaBH₈ were found to bond with B atoms in a manner that is similar to that in H₃S. Lattice dynamics calculations indicate that LaBH₇ and LaBH₈ become dynamically stable at pressures as low as 109.2 and 48.3 GPa, respectively. Moreover, the two phases were predicted to be superconducting with a critical temperature T_c of 93 K and 156 K at 110 GPa and 55 GPa, respectively ($\mu^*=0.1$). Our results provide guidance for future experiments targeting new hydride superconductors with both low synthesis pressures and high T_c .

I. INTRODUCTION

Exploration of superconductivity in materials at ever increasing temperatures is a burgeoning research topic in condensed matter physics, chemistry, and materials science. Conventional electron-phonon coupling considerations point to compressed hydrogen-rich materials as excellent candidates for superconductors having high critical temperatures (T_c 's) due to the potential for formation of atomic hydrogen lattices in which the low mass leads to both high vibrational frequencies and strong electron-phonon coupling. As originally proposed by Ashcroft¹, this concept has inspired numerous studies (see Refs.²⁻⁶ for reviews), specifically the recent progress on pressurized hydrides predicted and observed to have high T_c 's above 200 K in pursuit of superconductivity at, or even above, room temperature⁷⁻²². However, pressures in the megabar range (>100 GPa) are required to synthesize and stabilize the high- T_c hydrides considered so far. For example, high- T_c superconductivity was established above 170 and 166 GPa for clathrate metal hydrides LaH₁₀ and YH₆^{17,20}, and near 155 and 267 GPa for p -block element hydrides H₃S and C-S-H^{14,22}, respectively, where the pressures are those of the reported T_c maxima. Given the very high pressures required to create these high critical temperatures, the pursuit of high- T_c superconductivity in hydrides that can persist in stable

or metastable compounds at lower, and even ambient, pressure remains an important goal.

The stability of binary hydrides having potential superconducting T_c 's above 100 K has been largely limited to pressures above 100 GPa²³. For example, synthesis of superhydride UH₇ has been reported at a low pressure of 31 GPa, but its T_c is estimated to be 44 K^{24,25}. The lowest pressures reported for stabilization of a superhydride include those of CeH₉ at 80 GPa²⁶ and BaH₁₂ at 75 GPa²⁷ for atomic and molecular-based hydrogen structures, respectively. Predictions of lower pressure stability of hydrogen-rich binary hydrides include that of RbH₁₂, which is calculated to be stable at 50 GPa with a T_c near 115 K²³. With the additional degrees of freedom made possible by expanding the chemical space available, ternary hydrides are receiving growing interest as means both to increase T_c and to enhance stability over a broader range of pressures. As such, a T_c of 287 K has been reported in a C-S-H mixture at about 267 GPa, while the structure and composition for the high- T_c phase remain unclear²². Theoretical calculations predict that hydride perovskite structures based on the above elements could be a route to stabilizing lower pressure hydride superconductors, for example, by sublattice replacement of SH₃ with CH₄ in H₃S to produce structures of composition CSH₇ with predicted dynamical stability, and therefore kinetic stability, at lower pressures than that of pure H₃S^{28,29}. Lower level CH₄ substitution

in the material, either as stoichiometric compounds or doped structures, could enhance low-pressure stability, as well as significantly enhance T_c as recently predicted for the C-S-H superconductor³⁰. These results further suggest that ternary hydride systems may be a useful venue for discovering high- T_c superconductors at low pressures.

Metal hydrides having clathrate and related structures (e.g., MgH_6 , CaH_6 , YH_6 , LaH_{10} , and H_3S)^{7-10,12,13} have been predicted, and in several cases now observed, to have high T_c values that are higher than those with higher H content, such as MgH_{12} and MgH_{16} ³¹. This trend arises from the different forms of H atoms in the structures. In high- T_c hydrides, H_2 molecules accept electrons, inducing dissociation to form a monoatomic and metallic structure in which there is an increase the H contribution to the electronic states around the Fermi level and increasing the critical temperature. Therefore, the presence of atomic H in the structure is an important feature of high- T_c superconductivity of hydrides.

Theoretical studies indicate that adding Li and Ca to the B-H binary stabilizes phases that accommodate more atomic H atoms, leading to ternary hydrides with higher T_c 's relative to those found for B-H phases³²⁻³⁶. Given its larger ionic radius at ambient pressure, La can accommodate more atomic H (e.g., as a superhydride) compared to Li and Ca¹². Therefore, the stable phases with higher H content might be obtained in the La-B-H system under pressure. Moreover, a recent experimental study reported evidence for superconductivity at and above room temperature in La-hydride samples upon thermal annealing³⁷. Given that ammonia borane (NH_3BH_3) was used as a hydrogen source, the formation of La-H phases containing boron was suggested as giving rise to the high T_c ^{17,37}.

In this study, we examine theoretically high-pressure structures, stability, and superconducting properties of stoichiometric La-B-H phases, with a focus on lower pressure stability. Detailed study of phases with composition LaBH_x ($x=1-10$) and $\text{La}(\text{BH}_x)_3$ ($x=1-5$) reveals intriguing H-rich LaBH_7 ($P\bar{3}m1$) and LaBH_8 ($Fm\bar{3}m$) structures containing BH_6 and BH_8 units, respectively. Moreover, LaBH_7 and LaBH_8 are dynamically stable at pressures as low as 109.2 and 48.3 GPa, with predicted T_c 's of 93 and 156 K at 110 and 55 GPa, respectively. Our results indicate that continued exploration of ternary hydrides in these and related chemical systems may be an effective route to realizing a high-temperature superconductivity at lower, or even ambient, pressure.

II. COMPUTATIONAL DETAILS

The structure searches of La-B and La-B-H system were performed under pressure using the particle swarm optimization technique implemented in the CALYPSO code^{38,39}. The structural relaxations and electronic properties were calculated using density functional theory with the Perdew-Burke-Ernzerhof generalized gradient

approximation as implemented in the VASP code^{40,41}. The ion-electron interaction was described by projector-augmented-wave potentials, where $5s^25p^65d^16s^2$, $2s^22p^1$ and $1s^1$ configurations were treated as valence electrons for La, B and H atoms, respectively⁴². Plane wave kinetic energy cutoff was set to 700 eV and corresponding Monkhorst-Pack (MP) k -point meshes for different structures were adopted to ensure that the enthalpy converges to 1 meV/atom. Phonon calculations were performed by using the supercell method or density functional perturbation theory (DFPT) with PHONOPY⁴³ and Quantum-ESPRESSO codes⁴⁴, respectively. Electron-phonon coupling (EPC) calculations were carried out with the Quantum-ESPRESSO code using ultrasoft pseudopotentials for all atoms. We adopted a kinetic energy cutoff of 60 Ry. $7\times7\times5$, and $9\times9\times9$ q -point meshes in the first Brillouin zones (BZ) were used for $P\bar{3}m1$ - LaBH_7 and $Fm\bar{3}m$ - LaBH_8 , respectively. Correspondingly, we chose MP grids of $28\times28\times20$ and $36\times36\times36$ to ensure k -point sampling convergence.

III. RESULTS AND DISCUSSION

Before investigating the phase stability of ternary La-B-H compounds under pressure, we first assessed information about the La-H, B-H and La-B binaries. The high-pressure behavior of the B-H³⁴⁻³⁶ and La-H^{12,13,45-47} binaries has been well-studied in recent years, whereas information on the La-B system under pressure is lacking. We therefore performed structure-search calculations for La_nB_m ($n=1, m=1-8$; $n=2, m=1$) with system sizes containing up to 4 or 8 formula units (f.u.) per simulation cell at pressures of 0-300 GPa. To identify the stability of different stoichiometries, convex hulls were constructed by calculating the formation enthalpies for predicted La_nB_m structures relative to the elemental La and B (Fig. S1⁴⁸). All the stoichiometries were found to have negative formation enthalpies within 0-300 GPa, showing that they are thermodynamically stable with respect to decomposition into La and B elements. The increase in formation enthalpy indicates that the stability of the phase decreases with increasing pressure; in addition, a stoichiometry located on the hull is stable with respect to other binary compounds, otherwise it is metastable. **At 1 atm and 10 GPa, the experimentally observed LaB_4 and LaB_6 were predicted to be stable, which confirms the reliability of our method. At 50 GPa, with exception for LaB_4 and LaB_6 , a new stoichiometry LaB is also located on the convex hull. With increasing pressure to 100 GPa, we found that LaB , LaB_4 , LaB_5 and LaB_8 are stable, while LaB_6 was predicted to possibly decompose into $\text{LaB}_5+\text{LaB}_8$. At 200 GPa, only LaB and LaB_8 remain on the convex hull, and LaB_8 has the lowest formation enthalpy. At 300 GPa, LaB_8 remains stable, and LaB becomes metastable. The predicted stable structures of La-B compounds under pressure are shown in Fig. S2⁴⁸. In $R\bar{3}m$ - LaB , B atoms form graphene-**

like layers. With increasing B content, the B atoms are apt to form polyhedral configurations with decahedra in $Cmmm$ -LaB₄, octahedra in $P4/mmm$ -LaB₅ and octadecahedra in $R\bar{3}m$ -LaB₈, respectively.

Calculated La-B-H ternary phase diagrams at 100-300 GPa are presented in Fig. 1. All the ternary hydrides are stable relative to dissociation into elements at the pressures studied. Moreover, all the ternary hydrides LaBH_x studied have lower enthalpies than those of LaB and H₂, suggesting that they are stable against decomposition into LaB and H₂ (Fig. S3⁴⁸). We note that LaBH, LaBH₄, LaBH₆, La(BH)₃ and La(BH₄)₃ fall on the 3D convex hull at 100 GPa, indicating that they are also stable phases with respect to decomposition into binary and other ternary phases. At 150 GPa, an additional composition, LaBH₇, appears on the convex hull. With further increase in pressure to 200 GPa, the originally stable LaBH, LaBH₆ and La(BH₄)₃ are predicted to decompose into other compounds, and the higher H content LaBH₈ begins to become stable. At 300 GPa, the formation enthalpy of LaBH₈ is increasingly negative. LaBH₇ becomes metastable phases with higher enthalpies relative to $1/4$ LaBH₄+ $3/4$ LaBH₈. To determine accurate stability pressures, we also plot the specific enthalpy curves of LaBH₄, LaBH₆, LaBH₇ and LaBH₈ relative to other compounds (Fig. S4⁴⁸). After including zero-point energy corrections (Fig. S5⁴⁸)⁴⁹, we found that LaBH₄ remains thermodynamically stable in a $P2_1/m$ structure within the entire pressure range studied. $C2/c$ -LaBH₆ is stable below 134 GPa. For LaBH₇, the $P\bar{3}m1$ structure is predicted to become stable against dissociation into other stoichiometries at pressures of 103-233 GPa. LaBH₈ is predicted to crystallize in the cubic $Fm\bar{3}m$ structure, which is stable relative to LaBH₇ and H₂ above 161 GPa.

More recently, Cataldo *et al.*⁵⁰ reported simulations of the structure, superconductivity, and stability of LaBH₈. Although the results are largely consistent with our results, several differences should be noted. **First, Cataldo *et al.* predicted that $F\bar{4}3m$ -LaBH₅ and $Fm\bar{3}m$ -LaBH₈ are thermodynamically stable compositions at 100 and 110 GPa, respectively.** On the other hand, we find that $F\bar{4}3m$ -LaBH₅ and $Fm\bar{3}m$ -LaBH₈ are thermodynamically unstable with respect to decomposition into LaBH₄+LaBH₆ and LaBH₆+H₂ at 100 and 110 GPa, respectively. Relative enthalpy-pressure curves for LaBH₅ are shown in Fig. S6⁴⁸. Second, we found additional stoichiometries (LaBH, LaBH₄ and LaBH₆) to be stable at 100 GPa that were not mentioned in Ref.⁵⁰. In addition, we explored systematically the crystal structures of different stoichiometries and their stability at different pressures. Stable pressures of the predicted La-B-H compounds were determined that will provide clear guidance for experiments, including specific composition and structure information. Pressure favors the formation of more H-rich compounds in the La-B-H system, e.g., with LaBH₅, LaBH₆, LaBH₇ and LaBH₈, increasing stable under pressure. Finally, we point out interesting structural

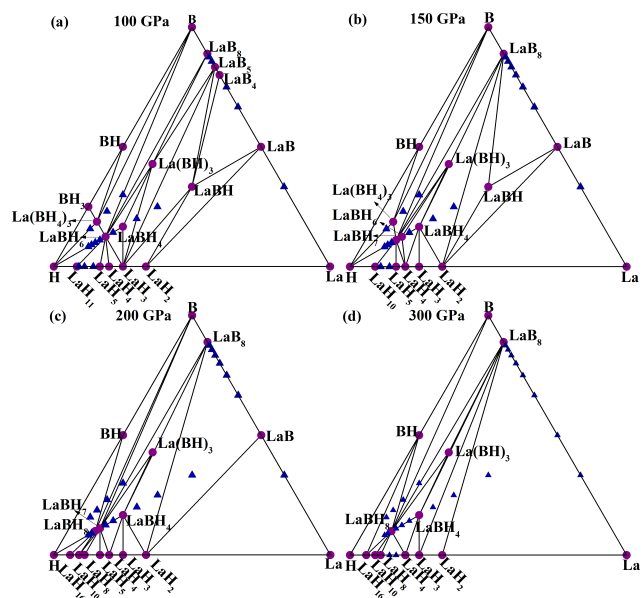


FIG. 1. Calculated convex hull of the La-B-H system is presented at 100, 150, 200 and 300 GPa, respectively. Thermodynamically stable and metastable stoichiometries are shown as purple circles and blue triangles, respectively.

trends among the La-B-H system are associated with this increase in H content. Specifically, the H atoms gradually bond with the surrounding B atoms, changing from BH units in LaBH₃ and LaBH₄ to BH₄ in LaBH₆, BH₆ in LaBH₇ and eventually BH₈ units in LaBH₈.

The predicted stable structures of the LaBH_x system are shown in Fig. 2. LaBH adopts the hexagonal $P6/mmm$ structure, in which B atoms form honeycomb sheets and B, La, and H atomic layers are alternately arranged. In LaBH₃ and LaBH₄, zigzag B chains stretch along specific directions while B atoms are surrounded by H atoms to form covalent bonds. Since more H atoms are filled in $C2/c$ -LaBH₆, no bonds exist between B atoms and each B atom forms a BH₄ unit with the adjacent four H atoms. With the increasing H content of LaBH₇, each B atom accommodates six H atom to form BH₆ units. The BH₆ groups are located on the vertices and edges of the hexagonal structure, with the BH₆ units distributed on the edges connected to each other by H atoms. The H-richer LaBH₈ assumes a high-symmetry $Fm\bar{3}m$ structure in which B atoms accommodate all the H atoms to form BH₈ covalent units that occupy the octahedral interstices of the face-centered cubic (fcc) lattice formed by La atoms. In H₃S, the S atoms located on a body-centered cubic lattice with each S atom covalently bonded to the surrounding six H atoms. The H atoms in LaBH₈ are found to bond with B in a manner that is similar to that of S in H₃S⁵¹. In addition, the atomic positions of La and eight H atoms in LaBH₈ are the same as those of La and eight of the H atoms in LaH₁₀. Given the high T_c of H₃S and LaH₁₀, this similarity in bonding and high symmetry structure suggests

interesting superconducting properties of LaBH_8 as well. The enthalpy curves and predicted stable structures of $\text{La}(\text{BH})_3$ and $\text{La}(\text{BH}_4)_3$ are shown in Fig. S7⁴⁸. $P\bar{1}$ - $\text{La}(\text{BH})_3$ is stable between 100-265 GPa and transforms to a Cm structure above 265 GPa. In $P\bar{1}$ - $\text{La}(\text{BH})_3$, B atoms bond to each other forming layered structures composed of 4- and 10- membered rings and H atoms locate between layers to bond with the surrounding B atoms. Cm $\text{La}(\text{BH})_3$ is an open-framework structure formed by B and H atoms with La-filled channels along the crystallographic b axis. $\text{La}(\text{BH}_4)_3$ is stable in the Cm structure between 100 and 150 GPa, where B atoms form chains and bond with surrounding H atoms. As a result, the remaining H atoms adopt the form of H_2 units. In addition, several metastable structures are also predicted as shown in Fig. S8⁴⁸.

At 100 GPa, the $F\bar{4}3m$ structure was predicted to have the lowest enthalpy in LaBH_5 , although it is metastable relative to other stoichiometries. As the pressure decreases to 50 GPa, the structure tends to become stable. As shown in Fig. S9⁴⁸, $F\bar{4}3m$ - LaBH_5 is constructed by fcc lattices formed by La atoms with BH_4 units and H atoms located on the octahedral and tetrahedral interstices respectively. $C2/c$ - LaBH_6 , which is stable at higher pressures, has a similar structure to $F\bar{4}3m$ - LaBH_5 but a little distorted, with more individual H atoms in the lattice. In LaBH_8 , a low-symmetry $P2_1/m$ structure is thermodynamically more favorable than the $Fm\bar{3}m$ structure below 154 GPa, where B atoms bond with seven H atoms forming BH_7 units. Under pressure, this structure will transform into more densely packed $Fm\bar{3}m$ structure with BH_8 units. This low-pressure $P2_1/m$ structure can be viewed as the distorted $Fm\bar{3}m$ structure. The La and B atoms always maintain NaCl-type structure in $F\bar{4}3m$ - LaBH_5 , $C2/c$ - LaBH_6 , $P2_1/m$ - LaBH_8 and $Fm\bar{3}m$ - LaBH_8 , showing that pressure has less effect on the La-B bonding. Moreover, these H-rich compounds have common structural features of B-H units, and the number of H atoms bonded to B increases with increasing pressure. To investigate the thermodynamic stability mechanism of $Fm\bar{3}m$ - LaBH_8 , we calculated the internal energies (U) and the pressure-volume (P - V) contributions to the enthalpy relative to LaBH_7+H_2 and $P2_1/m$ - LaBH_8 (Fig. S10⁴⁸). The P - V term of $Fm\bar{3}m$ - LaBH_8 is always lower than those of LaBH_7+H_2 and $P2_1/m$ - LaBH_8 , while U is opposite, showing that denser structure of cubic $Fm\bar{3}m$ - LaBH_8 is the key factor for its stability.

Lattice dynamics calculations were carried out for the phases in the pressure ranges of their predicted thermodynamic stability. The lack of imaginary frequencies in the calculated phonon dispersion curves indicates that all structures are dynamically stable within the harmonic approximation (Figs 5 and S11⁴⁸). On the other hand, phonon softening is evident for LaBH_7 and LaBH_8 , an effect that can enhance the EPC¹². With decreasing pressure, these phonon modes further soften and eventually have imaginary frequencies. Figure S12⁴⁸ shows the fre-

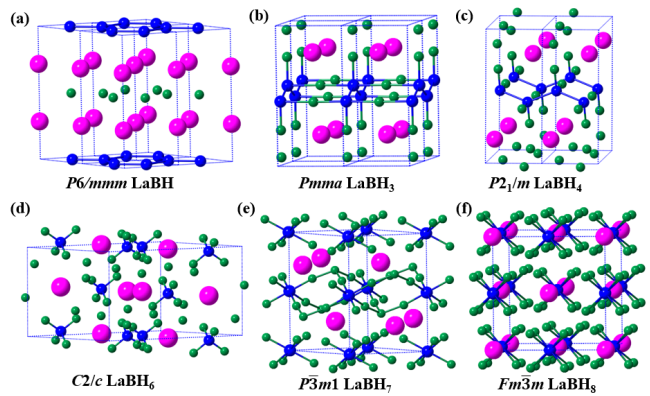


FIG. 2. The predicted crystal structures of ternary hydrides under pressure. (a) $P6/mmm$ - LaBH , (b) $Pmma$ - LaBH_3 , (c) $P2_1/m$ - LaBH_4 , (d) $C2/c$ - LaBH_6 , (e) $P\bar{3}m1$ - LaBH_7 and (f) $Fm\bar{3}m$ - LaBH_8 . Magenta, blue and green balls represent La, B and H atom, respectively.

quency of the softest mode as a function of pressure. In contrast to LaH_{10} , however, LaBH_7 and LaBH_8 maintain dynamical stability to pressures as low as 109.2 and 48.3 GPa, respectively, the latter being much lower than that predicted for other H-rich hydride superconductors.

To understand the origin of relatively low-pressure stability of $P\bar{3}m1$ - LaBH_7 and $Fm\bar{3}m$ - LaBH_8 , we explored the bonding of these structures by calculating the electron localization function (ELF)^{52,53} and Bader charge transfer⁵⁴ among atoms. ELF with an isosurface of 0.6 are shown in Figs 3a and b for the two phases at 110 and 55 GPa, respectively. Electron density at the La atoms is due to their inner valence shells. Many electrons are clearly localized between B and H atoms and closer to the H atoms. The ELF slice in the (110) plane containing La, B and H atoms for LaBH_7 and LaBH_8 (Fig. 3c) also shows that the ELF values between B and H atoms gradually increase toward H atoms, suggesting the polar covalent character of the B-H bond. For comparison, we calculated the ELF of the well-known hydrogen storage material LiBH_4 at 1atm (Fig. S13⁴⁸), which contains a strong BH_4 covalent unit. The ELF values around B and between B and H atoms in LaBH_7 and LaBH_8 are similar to those in LiBH_4 . As shown in Fig. S9⁴⁸, the bond lengths of the B-H bonds in La-B-H compounds are comparable to those of 1.23 Å in LiBH_4 at 1 atm. Moreover, similar results were also found in $Im\bar{3}m$ - H_3S ⁷. In LaBH_7 , atom H_2 appears to form a covalent bond to H_1 with an ELF value of 0.64 connecting BH_6 units on the edges. In both phases, the ELF values at the center of the shortest La-H and La-B are below 0.3, indicative of an ionic character between La and B-H units.

To provide a deeper insight into the bonding, we calculated the Crystal Orbital Hamilton Population (COHP) and its integration ICOHP⁵⁵⁻⁵⁷ projected onto B-H and H-H pairs in LaBH_7 and LaBH_8 at different pressures, and H-S bonds in H_3S at 200 GPa for comparison. Positive and negative -COHP indicate bonding and anti-

bonding interactions, respectively. The ICOHP up to the Fermi level can describe the atom pair interaction strength. Fig. S14⁴⁸ clearly shows there are strong B-H bonding states below the Fermi level in LaBH₇ and LaBH₈, which are similar to the case of H-S in H₃S. The H1-H2 interaction in LaBH₇ is weak and mainly distributed around 10 eV below the Fermi energy, while the interaction strength of H2-H3 in LaBH₇ and H-H in LaBH₈ are negligible, which suggests that the H-H bond will not play a major role in structural stability and properties. The -ICOHP at the Fermi level increases with pressure, which indicates the enhancement of the B-H interactions. At 200 GPa, the calculated -ICOHP between B and H atoms at Fermi level are 3.34 and 3.18 in LaBH₇ and LaBH₈, values that are comparable to that of 3.50 between S and H in H₃S, indicating the H atoms in LaBH₇ and LaBH₈ bond with B in a manner as H-S in H₃S.

Bader charge calculations show that electrons transfer from La and B to H atoms. In LaBH₇, each La atom and B atom located on the vertex and edge of the lattice loses 1.44, 1.37 and 1.16 electrons, respectively. Correspondingly, each H atom in BH₆ at the vertex (H3) and edge (H1) accepts 0.45 and 0.39 electrons, respectively. The H atom (H2) that only bonds with a H atom gets 0.15 electrons. The existence of the H1-H2 covalent bond weakens the B-H1 bond connected to it. In LaBH₈, each La and B atom transfers 1.47 and 1.04 electrons to eight H atoms, respectively. With increasing pressure, the number of electrons transferred by La and B atom decreases and increases, respectively. *Fm* $\bar{3}$ *m*-LaBH₈ possesses the same fcc lattices composed by La atoms as in *Fm* $\bar{3}$ *m*-LaH₁₀. The difference is that B and H atoms form strong covalent bonds in LaBH₈, while the H atoms in LaH₁₀ are connected by weak covalent bonds forming a cage structure. At 200 GPa, the calculated -ICOHP for the B-H bond in LaBH₈ is 3.18, which is much higher than 0.17 for the H-H bond, revealing strong interactions between B and H atoms in LaBH₈. The calculated -ICOHP for H-H pairs in LaH₁₀ (Fig. S15⁴⁸) is 1.6, showing weak covalent bonds. By analyzing the eigenvectors of soft modes for LaBH₈ and LaH₁₀, it is found that their structural stabilities are mainly associated with the vibrations of the B-H and H-H bond, respectively (Fig. S16⁴⁸). With decreasing pressure, the distance between atoms becomes longer and the interactions weaker, which eventually leads to a structural instability and phase transition (Fig. S17⁴⁸)^{12,45}. The results indicated that the B-H bonds in LaBH₈ are much stronger than H-H interactions in LaH₁₀, and the B and H atoms can maintain a bonding interaction over large pressure range. Therefore, the strong interactions between B and H atoms play an important role in determining its relatively low-pressure dynamical stability.

We further investigated the electronic properties of the stable structures found in the La-B-H system. The calculated electronic density of states (DOS) for *P6/mmm*-LaBH, *Pmma*-LaBH₃, *P2₁/m*-LaBH₄ and *C2/c*-LaBH₆

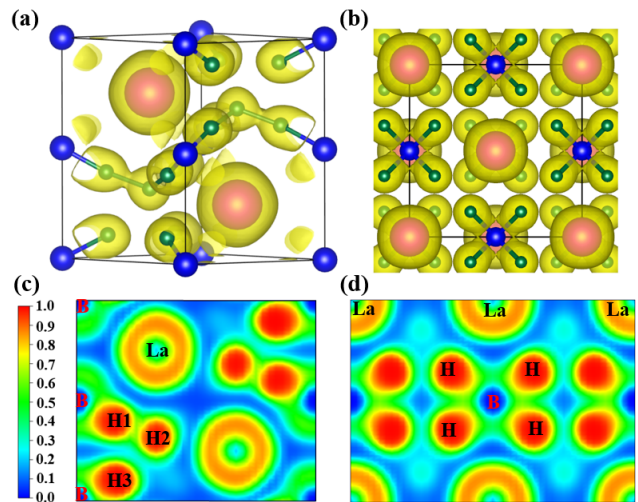


FIG. 3. The Calculated ELF with isosurface value of 0.6 and ELF in the (1 1 0) plane for (a) *P* $\bar{3}$ *m*1-LaBH₇ and (b) *Fm* $\bar{3}$ *m*-LaBH₈ at 110 and 55 GPa, respectively.

within their ranges of pressure stability are shown in Fig. S18⁴⁸. The electronic DOS at the Fermi level indicates that they are all metallic. *P6/mmm*-LaBH, *Pmma*-LaBH₃ and *P2₁/m*-LaBH₄ all have relatively high DOS values at the Fermi level. However, this metallicity is mainly derived from the contribution of La and B atoms: there is a negligible H contribution to the DOS at Fermi level, which is unfavorable to superconductivity. In *C2/c*-LaBH₆, the Fermi level falls at the valley of the electronic DOS, showing poor metallicity.

We further focused our investigation on the H-richer LaBH₇ and LaBH₈ compounds. Figure 4 illustrates the calculated electronic band structures, DOS and Fermi surface of *P* $\bar{3}$ *m*1-LaBH₇ and *Fm* $\bar{3}$ *m*-LaBH₈ at 110 and 55 GPa, respectively. They are the metallic phases with some bands crossing the Fermi level. In LaBH₇, a flat band with more localized electronic states appears near the Fermi level at the Γ point, which might enhance the electron-phonon interactions. Flat-steep band features are beneficial for superconductivity⁵⁸. As such, the steep and flat bands are found for LaBH₈ along the Γ -X and X-W directions near the Fermi level, respectively. According to the calculated ELFs, the distributions of ELF between H2 and H3 in LaBH₇ and H atoms in neighboring BH₈ units in LaBH₈ can be seen as the picture of two tangent circles, respectively. The ELF values decrease gradually from the center of one atom to the middle point of the two atoms. Therefore, we roughly considered half of the distance between H2 and H3 in LaBH₇ and H atoms in neighboring BH₈ units in LaBH₈ as the H projected radius for the projected DOS calculations. The results show that the contribution of H atoms to the DOS at the Fermi level exceeds that of La and B atoms in LaBH₇, and the metallicity are dominated by H atoms in LaBH₈, which suggest that *P* $\bar{3}$ *m*1-LaBH₇ and *Fm* $\bar{3}$ *m*-LaBH₈ may be high-*T_c* superconductors. Both the Fermi

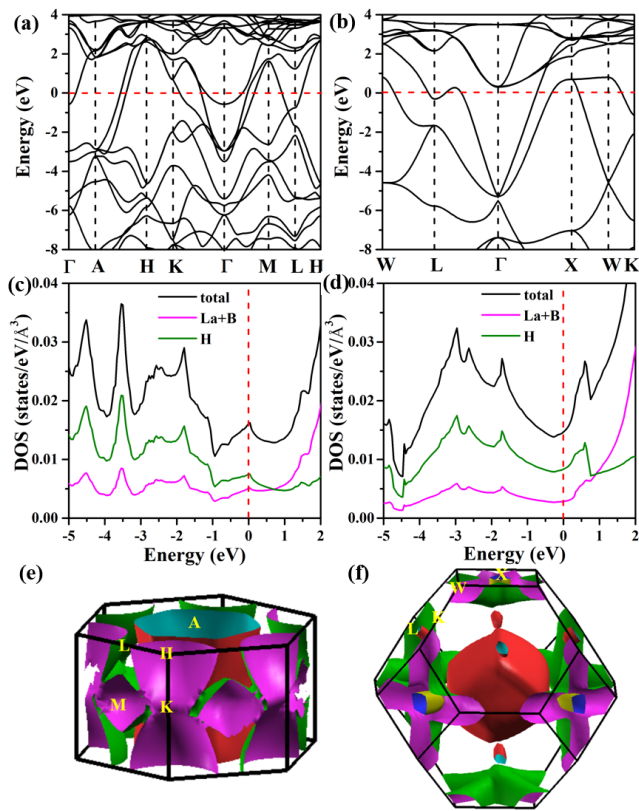


FIG. 4. The calculated electronic band structure, density of states and Fermi surfaces of $P\bar{3}m1$ -LaBH₇ and $Fm\bar{3}m$ -LaBH₈ at 110 and 55 GPa, respectively.

surfaces of $P\bar{3}m1$ -LaBH₇ and $Fm\bar{3}m$ -LaBH₈ are composed of three sheets and one of them is an electronlike ellipsoid and polyhedron around the Γ point respectively. In LaBH₇, one Fermi surface sheet is like a tube along the Γ -A direction and the other is distributed in a large outer region of the Brillouin zone. In LaBH₈, with the exception of a cross-like sheet, there are small electron and hole pockets at L and X point, respectively.

Given their promising electronic properties, we calculated the superconducting properties of LaBH₇ and LaBH₈. We calculated their phonon spectra, projected phonon DOS, Eliashberg phonon spectral function $\alpha^2 F(\omega)/\omega$ and integral $\lambda(\omega)$ for the two phases at 110 and 200 GPa, respectively (Fig. 5a, b). Similar to the hydrides studied previously, the projected phonon DOS can be separated into three regions. The La atom with the heaviest atomic mass dominates the low-frequency region, whereas the vibrations of the B and H atoms are associated with the mid- and high-frequency phonon branches, respectively. The spectral function $\alpha^2 F(\omega)/\omega$ for LaBH₇ is mainly distributed below 30 THz, especially between 8-15 THz (Fig. 5a), which results in an EPC constant λ of 1.46 at 110 GPa. However, the value of the phonon DOS between 8-15 THz is negligible. Further analysis reveals a soft mode in this frequency range with a potentially large EPC contribution. The distribution of

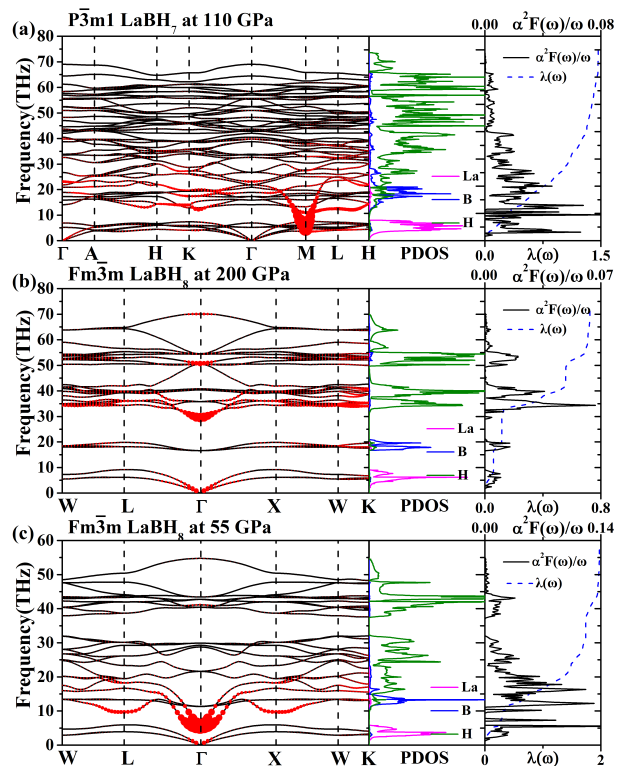


FIG. 5. Calculated phonon dispersion curves (red circle area proportional to associated EPC), projected phonon density of states (PDOS), the Eliashberg phonon spectral function $\alpha^2 F(\omega)/\omega$ and its integral $\lambda(\omega)$ of (a) $P\bar{3}m1$ -LaBH₇ at 110 GPa, (b) $Fm\bar{3}m$ -LaBH₈ at 200 GPa and (c) $Fm\bar{3}m$ -LaBH₈ at 55 GPa.

the EPC strength on the different phonon modes are also plotted with the spectra. The soft mode associated to H atoms below 20 THz around the M point shows a quite large EPC. Similarly, for LaBH₈ the calculated EPC λ is 0.72 at 200 GPa, and the contribution to λ of the vibrations related to H atoms above 30 THz accounts for 83% of the total value. The soft mode near 30 THz at Γ point makes an important contribution to the EPC. Previous studies of related superconducting hydrides indicate that the total EPC may be enhanced by further phonon softening induced by decompression toward the structural instability predicted by this harmonic approximation of the lattice dynamics^{7,12}. Calculations for LaBH₈ indicate that λ increases to 1.97 and 2.29 near its predicted instability at 55 (Fig. 5c) and 50 GPa (Fig. S19⁴⁸), which are comparable with the value of 2.19 found for H₃S at 200 GPa. As discussed above, our results show that the interaction between B and H atoms is stronger than that between H atoms in LaBH₈. **The contribution to the strong EPC at 55 GPa arising from soft modes (5-20 THz) is about 59 %, which is mainly associated with the vibrations of B-H and H-H (Figure 5c).**

We adopted the Allen-Dynes modified McMillan equation to estimate the T_c of $P\bar{3}m1$ -LaBH₇ and $Fm\bar{3}m$ -LaBH₈ at different pressures (Table 1)⁵⁹. For LaBH₇,

TABLE I. The calculated electron-phonon coupling parameter λ , phonon frequency logarithmic average ω_{log} and critical temperature T_c ($\mu^*=0.1-0.13$) from Allen-Dynes modified McMillan, McMillan with the strong-coupling and the shape corrections (f_1 and f_2) and Eliashberg equations for $P\bar{3}m1$ -LaBH₇ and $Fm\bar{3}m$ -LaBH₈.

	P (GPa)	λ	ω_{log} (K)	T_c (K) McMillan	T_c (K) McMillan(f_1 and f_2)	T_c (K) Eliashberg
				$\mu^*=0.1-0.13$	$\mu^*=0.1-0.13$	$\mu^*=0.1$
LaBH ₇ ($P\bar{3}m1$)	110	1.46	837	93-85	–	–
LaBH ₈ ($Fm\bar{3}m$)	200	0.72	1557	58-45	–	–
LaBH ₈ ($Fm\bar{3}m$)	100	1.11	1189	96-84	–	–
LaBH ₈ ($Fm\bar{3}m$)	55	1.97	807	115-107	127-139	156
LaBH ₈ ($Fm\bar{3}m$)	50	2.29	692	108-102	126-138	154

the calculated λ and phonon frequency logarithmic average ω_{log} is 1.46 and 837 K at 110 GPa, leading to a T_c of 93 K with $\mu^*=0.1$. As pressure decreases from 200 to 100, 55 and 50 GPa, the calculated λ for LaBH₈ increases from 0.72 to 1.11, 1.97 and 2.29, whereas ω_{log} decreases from 1557 to 1189, 807 and 692 K. As a result of these two effects, the calculated T_c first increases from 58 to 115 K and then decreases to 108 K assuming $\mu^*=0.1$, which follows the trend of λ and with pressure, respectively. Since the λ of LaBH₈ at 55 and 50 GPa are much greater than 1.5, the accuracy of T_c values was improved by considering the strong-coupling and the shape corrections (f_1 and f_2). The estimated T_c values are 139 and 138 K with $\mu^*=0.1$. By numerically solving the Eliashberg equation⁶⁰, the T_c s increase a little, becoming 156 and 154 K, respectively.

IV. CONCLUSIONS

Density functional theory-based structure-search calculations have identified seven phases in the ternary La-B-H system at pressures of 100-300 GPa that are potential targets for experimental synthesis. Most significant

are the predictions of stability of H-rich $P\bar{3}m1$ -LaBH₇ at 103-223 GPa and $Fm\bar{3}m$ -LaBH₈ above 161 GPa, with the latter calculated to be dynamically stable as low as 48.3 GPa. Structural trends among these phases are observed as the H content increases. In LaBH, the B atoms form graphene-like layers, whereas in LaBH₃ and LaBH₄, the B atoms not only bond with each other to form zigzag chains, but bond with H atoms. In LaBH₆ and LaBH₇, there are no B-B bonds and B atoms are coordinated by Hs to form BH₄ and BH₆ units. LaBH₈ is stable in the high-symmetry $Fm\bar{3}m$ structure, in which the B atoms accommodate all the H atoms to form BH₈ units. The La atom acts as an electron donor in the structures to stabilize the higher H content B-H units. Moreover, EPC calculations show that LaBH₇ and LaBH₈ are potential superconductors. Softening of phonons dominated by H-atom vibrations in these structures makes a large contribution to superconductivity. The estimated T_c of LaBH₇ is 93 K at 110 GPa, whereas the T_c of LaBH₈ is calculated to be as high as 156 K at 55 GPa. The expanded range of dynamical stability to low pressures together with its predicted relatively high T_c make $Fm\bar{3}m$ -LaBH₈ a promising candidate superconductor for low-pressure stabilization experiments. Similar results for LaBH₈ were reported during the preparation and submission of this manuscript^{50,61,62}. Additional chemical substitution of these phases could be used to enhance both T_c (e.g., by electron or hole doping) or structural stability at still lower pressures. Additional theoretical work could explore potential anharmonic and quantum effects on the stability and the calculated critical temperatures^{45,46,63}. The present study is thus expected to stimulate further research on ternary and more complex superconducting hydrides with high critical temperatures and expanded ranges of stability.

ACKNOWLEDGMENTS

The work was supported by National Natural Science Foundation of China (No. 52022089, 11874076, 12074138), and the Ph.D. Foundation by Yanshan University (Grant No. B970). A.B. acknowledges financial support from the Spanish Ministry of Science and Innovation (Grant No. FIS2019-105488GB-I00). R.H. acknowledges support from the U.S. National Science Foundation (DMR-1933622).

* hanyuliu@jlu.edu.cn

† gaoguoying@ysu.edu.cn

¹ N. W. Ashcroft, Phys. Rev. Lett. **92**, 187002 (2004).

² H. Wang, X. Li, G. Gao, Y. Li, and Y. Ma, WIREs: Comput. Mol. Sci. : Comput. Mol. Sci. **8**, e1330 (2018).

³ E. Zurek and T. Bi, J Chem. Phys. **150**, 050901 (2019).

⁴ J. A. Flores-Livas, L. Boeri, A. Sanna, G. Profeta, R. Arita, and M. Eremets, Phys. Rep. **856**, 1 (2020).

⁵ D. V. Semenov, I. A. Kruglov, I. A. Savkin, A. G. Kvashnin, and A. R. Oganov, Curr. Opin. Solid State Mater. Sci. **24**, 100808 (2020).

⁶ C. J. Pickard, I. Errea, and M. I. Eremets, Annu. Rev. Condens. Matter Phys. **11**, 57 (2020).

⁷ D. Duan, Y. Liu, F. Tian, D. Li, X. Huang, Z. Zhao, H. Yu, B. Liu, W. Tian, and T. Cui, Sci. Rep. **4**, 6968 (2014).

- ⁸ H. Wang, J. S. Tse, K. Tanaka, T. Iitaka, and Y. Ma, Proc. Natl. Acad. Sci. U.S.A. **109**, 6463 (2012).
- ⁹ Y. Li, J. Hao, H. Liu, J. Tse, Y. Wang, and Y. Ma, Sci. Rep. **5**, 9948 (2015).
- ¹⁰ X. Feng, J. Zhang, G. Gao, H. Liu, and H. Wang, RSC adv. **5**, 59292 (2015).
- ¹¹ X. Liang, A. Bergara, L. Wang, B. Wen, Z. Zhao, X.-F. Zhou, J. He, G. Gao, and Y. Tian, Phys. Rev. B **99**, 100505(R) (2019).
- ¹² H. Liu, I. I. Naumov, R. Hoffmann, N. W. Ashcroft, and R. J. Hemley, Proc. Natl. Acad. Sci. U.S.A. **114**, 6990 (2017).
- ¹³ F. Peng, Y. Sun, C. J. Pickard, R. J. Needs, Q. Wu, and Y. Ma, Phys. Rev. Lett. **119**, 107001 (2017).
- ¹⁴ A. P. Drozdov, M. I. Erements, I. A. Troyan, V. Ksenofontov, and S. I. Shylin, Nature **525**, 73 (2015).
- ¹⁵ M. Einaga, M. Sakata, T. Ishikawa, K. Shimizu, M. Erements, A. Drozdov, I. Troyan, N. Hirao, and Y. Ohishi, Nat. Phys. **12**, 835 (2016).
- ¹⁶ Z. M. Geballe, H. Liu, A. K. Mishra, M. Ahart, M. Somayazulu, Y. Meng, M. Baldini, and R. J. Hemley, Angew. Chem. Int. Ed. **57**, 688 (2018).
- ¹⁷ M. Somayazulu, M. Ahart, A. K. Mishra, Z. M. Geballe, M. Baldini, Y. Meng, V. V. Struzhkin, and R. J. Hemley, Phys. Rev. Lett. **122**, 027001 (2019).
- ¹⁸ A. Drozdov, P. Kong, V. Minkov, S. Besedin, M. Kuzovnikov, S. Mozaffari, L. Balicas, F. Balakirev, D. Graf, V. Prakapenka, *et al.*, Nature **569**, 528 (2019).
- ¹⁹ P. Kong, V. Minkov, M. Kuzovnikov, S. Besedin, A. Drozdov, S. Mozaffari, L. Balicas, F. Balakirev, V. Prakapenka, E. Greenberg, *et al.*, arXiv:1909.10482 (2019).
- ²⁰ I. A. Troyan, D. V. Semenov, A. G. Kvashnin, A. V. Sadakov, O. A. Sobolevskiy, V. M. Pudalov, A. G. Ivanova, V. B. Prakapenka, E. Greenberg, A. G. Gavriliuk, *et al.*, Adv. Mater. **33**, 2006832 (2021).
- ²¹ D. V. Semenov, A. G. Kvashnin, A. G. Ivanova, V. Svitlyk, V. Y. Fominski, A. V. Sadakov, O. A. Sobolevskiy, V. M. Pudalov, I. A. Troyan, and A. R. Oganov, Mater. Today **33**, 36 (2020).
- ²² E. Snider, N. Dasenbrock-Gammon, R. McBride, M. Debessai, H. Vindana, K. Venkatasamy, K. V. Lawler, A. Salamat, and R. P. Dias, Nature **586**, 373 (2020).
- ²³ M. J. Hutcheon, A. M. Shipley, and R. J. Needs, Phys. Rev. B **101**, 144505 (2020).
- ²⁴ I. A. Kruglov, A. G. Kvashnin, A. F. Goncharov, A. R. Oganov, S. S. Lobanov, N. Holtgrewe, S. Jiang, V. B. Prakapenka, E. Greenberg, and A. V. Yanilkin, Sci. Adv. **4**, eaat9776 (2018).
- ²⁵ B. Guigue, A. Marizy, and P. Loubeyre, Phys. Rev. B **102**, 014107 (2020).
- ²⁶ N. P. Salke, M. M. D. Esfahani, Y. Zhang, I. A. Kruglov, J. Zhou, Y. Wang, E. Greenberg, V. B. Prakapenka, J. Liu, A. R. Oganov, *et al.*, Nature Commun. **10**, 1 (2019).
- ²⁷ W. Chen, D. V. Semenov, A. G. Kvashnin, X. Huang, I. A. Kruglov, M. Galasso, H. Song, D. Duan, A. F. Goncharov, V. B. Prakapenka, *et al.*, Nature Commun. **12**, 1 (2021).
- ²⁸ W. Cui, T. Bi, J. Shi, Y. Li, H. Liu, E. Zurek, and R. J. Hemley, Phys. Rev. B **101**, 134504 (2020).
- ²⁹ Y. Sun, Y. Tian, B. Jiang, X. Li, H. Li, T. Iitaka, X. Zhong, and Y. Xie, Phys. Rev. B **101**, 174102 (2020).
- ³⁰ Y. Ge, F. Zhang, R. P. Dias, R. J. Hemley, and Y. Yao, Mater. Today Phys. **15**, 100330 (2020).
- ³¹ D. C. Lonie, J. Hooper, B. Altintas, and E. Zurek, Phys. Rev. B **87**, 054107 (2013).
- ³² C. Kokail, W. von der Linden, and L. Boeri, Phys. Rev. Mater. **1**, 074803 (2017).
- ³³ S. Di Cataldo, W. von der Linden, and L. Boeri, Phys. Rev. B **102**, 014516 (2020).
- ³⁴ C.-H. Hu, A. R. Oganov, Q. Zhu, G.-R. Qian, G. Frapper, A. O. Lyakhov, and H.-Y. Zhou, Phys. Rev. Lett. **110**, 165504 (2013).
- ³⁵ Y. Yao and R. Hoffmann, J. Am. Chem. Soc. **133**, 21002 (2011).
- ³⁶ W.-H. Yang, W.-C. Lu, S.-D. Li, X.-Y. Xue, Q.-J. Zang, K.-M. Ho, and C.-Z. Wang, Phys. Chem. Chem. Phys. **21**, 5466 (2019).
- ³⁷ A. Grockowiak, M. Ahart, T. Helm, W. Coniglio, R. Kumar, M. Somayazulu, Y. Meng, M. Oliff, V. Williams, N. Ashcroft, *et al.*, arXiv:2006.03004 (2020).
- ³⁸ Y. Wang, J. Lv, L. Zhu, and Y. Ma, Phys. Rev. B **82**, 094116 (2010).
- ³⁹ Y. Wang, J. Lv, L. Zhu, and Y. Ma, Comput. Phys. Commun. **183**, 2063 (2012).
- ⁴⁰ G. Kresse and J. Furthmüller, Phys. Rev. B **54**, 11169 (1996).
- ⁴¹ J. P. Perdew, J. A. Chevary, S. H. Vosko, K. A. Jackson, M. R. Pederson, D. J. Singh, and C. Fiolhais, Phys. Rev. B **46**, 6671 (1992).
- ⁴² P. E. Blüchl, Phys. Rev. B **50**, 17953 (1994).
- ⁴³ A. Togo, F. Oba, and I. Tanaka, Phys. Rev. B **78**, 134106 (2008).
- ⁴⁴ P. Giannozzi, S. Baroni, N. Bonini, M. Calandra, R. Car, C. Cavazzoni, D. Ceresoli, G. L. Chiarotti, M. Cococcioni, and I. Dabo, J. Phys.: Condens. Matter **21**, 395502 (2009).
- ⁴⁵ H. Liu, I. I. Naumov, Z. M. Geballe, M. Somayazulu, S. T. John, and R. J. Hemley, Phys. Rev. B **98**, 100102(R) (2018).
- ⁴⁶ I. Errea, F. Belli, L. Monacelli, A. Sanna, T. Koretsune, T. Tadano, R. Bianco, M. Calandra, R. Arita, F. Mauri, *et al.*, Nature **578**, 66 (2020).
- ⁴⁷ I. A. Kruglov, D. V. Semenov, H. Song, R. Szczesniak, I. A. Wrona, R. Akashi, M. M. D. Esfahani, D. Duan, T. Cui, A. G. Kvashnin, *et al.*, Phys. Rev. B **101**, 024508 (2020).
- ⁴⁸ See Supplemental Material at *** for formation enthalpies per atom of La_nB_m and LaBH_x ($x=1-10$) at 100-300 GPa, the predicted stable structures of La-B system under pressure, relative enthalpy-pressure curves for LaBH_4 , LaBH_6 , LaBH_7 and LaBH_8 relative to the corresponding binary hydrides as a function of pressure without and with zero-point energy, the enthalpy curves of structures for LaBH_5 relative to other ternary La-B-H compounds as a function of pressure, the enthalpy curves and predicted stable structures of $\text{La}(\text{BH})_3$ and $\text{La}(\text{BH}_4)_3$, crystal structures of several predicted metastable La-B-H compounds, crystal structures of $F\bar{4}3m$ - LaBH_5 , $C2/c$ - LaBH_6 , $P2_1/m$ - LaBH_8 and $Fm\bar{3}m$ - LaBH_8 , calculated internal energies U and PV components of the enthalpy of the $Fm\bar{3}m$ - LaBH_8 , phonon dispersion relations for the predicted stable structures at different pressures, the calculated frequency of the softest mode of LaBH_7 and LaBH_8 as a function of pressure, calculated ELF of $Pnma$ LiBH_4 and $Im\bar{3}m$ - H_3S , the calculated COHP and its integration ICOHP for B-H and H-H pairs in LaBH_7 and LaBH_8 and H-S in H_3S at different pressures; the calculated COHP and its integration ICOHP for H-H pairs in LaH_{10} , eigenvectors of the soft phonon modes in LaBH_7 , LaBH_8 and LaH_{10} , the calculated B-H, H-H distances as a function of pressure for LaBH_8 , LiBH_4 and LaH_{10} , electronic density of states (DOS) of predicted

- stable LaBH, LaBH₃, LaBH₄ and LaBH₆ at their stable pressures, superconductivity of LaBH₈ at 50 GPa, detailed structural parameters of the predicted La-B compounds and La-B-H ternary hydrides.
- ⁴⁹ Y. Ma and S. T. John, *Solid State Commun.* **143**, 161 (2007).
- ⁵⁰ S. Di Cataldo, C. Heil, W. von der Linden, and L. Boeri, *Phys. Rev. B* **104**, L020511 (2021).
- ⁵¹ N. Bernstein, C. S. Hellberg, M. D. Johannes, I. I. Mazin, and M. J. Mehl, *Phys. Rev. B* **91**, 060511 (2015).
- ⁵² A. D. Becke and K. E. Edgecombe, *J Chem. Phys.* **92**, 5397 (1990).
- ⁵³ A. Savin, O. Jepsen, J. Flad, O. K. Andersen, H. Preuss, and H. G. von Schnering, *Angew. Chem. Int. Ed.* **31**, 187 (1992).
- ⁵⁴ R. Bader, *Atoms in Molecules: A Quantum Theory* (Oxford University Press, 1994).
- ⁵⁵ R. Dronskowski and P. E. Bloechl, *J Phys. Chem.* **97**, 8617 (1993).
- ⁵⁶ V. L. Deringer, A. L. Tchougréeff, and R. Dronskowski, *The journal of physical chemistry A* **115**, 5461 (2011).
- ⁵⁷ S. Maintz, V. L. Deringer, A. L. Tchougréeff, and R. Dronskowski, “Lobster: A tool to extract chemical bonding from plane-wave based dft,” (2016).
- ⁵⁸ A. Simon, *Angew. Chem. Int. Ed.* **36**, 1788 (1997).
- ⁵⁹ P. B. Allen and R. C. Dynes, *Phys. Rev. B* **12**, 905 (1975).
- ⁶⁰ G. Eliashberg, *Sov. Phys. JETP* **11**, 696 (1960).
- ⁶¹ Z. Zhang, T. Cui, M. J. Hutcheon, A. M. Shipley, H. Song, M. Du, V. Z. Kresin, D. Duan, C. J. Pickard, and Y. Yao, arXiv preprint arXiv:2106.09879 (2021).
- ⁶² S. Di Cataldo, W. von der Linden, and L. Boeri, arXiv preprint arXiv:2106.07266 (2021).
- ⁶³ H. Wang, Y. Yao, F. Peng, H. Liu, and R. J. Hemley, *Phys. Rev. Lett.* **126**, 117002 (2021).